

# Journal of Materials Chemistry A

Accepted Manuscript



This is an *Accepted Manuscript*, which has been through the Royal Society of Chemistry peer review process and has been accepted for publication.

*Accepted Manuscripts* are published online shortly after acceptance, before technical editing, formatting and proof reading. Using this free service, authors can make their results available to the community, in citable form, before we publish the edited article. We will replace this *Accepted Manuscript* with the edited and formatted *Advance Article* as soon as it is available.

You can find more information about *Accepted Manuscripts* in the [Information for Authors](#).

Please note that technical editing may introduce minor changes to the text and/or graphics, which may alter content. The journal's standard [Terms & Conditions](#) and the [Ethical guidelines](#) still apply. In no event shall the Royal Society of Chemistry be held responsible for any errors or omissions in this *Accepted Manuscript* or any consequences arising from the use of any information it contains.

**New insights into multi-shape memory behaviours and liquid crystalline properties of supramolecular polyurethane complexes based on pyridine-containing polyurethane and 4-n-Octyldecyloxybenzoic acid**

Shaojun Chen<sup>1</sup>, Funian Mo<sup>1</sup>, Shiguo Chen<sup>1</sup>, Zaochuan Ge<sup>1</sup>, Haipeng Yang<sup>1</sup>, Jiandong Zuo<sup>1</sup>, Xinke Liu<sup>1\*</sup>, Haitao Zhuo<sup>2\*</sup>,

<sup>1</sup>Shenzhen Key Laboratory of Special Functional Materials, Nanshan District Key Lab for Biopolymers and Safety Evaluation, College of Materials Science and Engineering, Shenzhen University, Shenzhen, 518060, China. <sup>2</sup> College of Chemistry and Chemical Engineering, Shenzhen University, Shenzhen, 518060, China.

Corresponding authors: College of Materials Science and Engineering, Shenzhen University, Shenzhen, 518060, China. E-mail: X.K. Liu [xkliu@szu.edu.cn](mailto:xkliu@szu.edu.cn); H.T.Zhuo, [haitaozhuo@163.com](mailto:haitaozhuo@163.com)

**Abstract**

Liquid crystalline polymers and shape memory polymers are both attractive to researchers. This paper describes the development of a supramolecular liquid crystalline complex exhibiting a multi-shape memory effect and liquid crystalline properties. 4-n-Octyldecyloxybenzoic acid (OOBA) is connected to a pyridine-containing polyurethane (PySMPU), forming a new PySMPU/OOBA complex. The results of this study demonstrate that the complex maintains the intrinsic crystallization and liquid-crystalline properties of OOBA and combines the shape memory effects of PySMPUs. Shape memory investigations demonstrate that the PySMPU/OOBA complexes have a good multi-shape memory effect, exhibiting triple- and quadruple-shape memory behaviours. For the triple-shape memory behaviours, the strain fixity at the first stage is lower than that at the second stage, while the strain recovery at the first stage is higher than that at the second stage. Overall, increasing the OOBA content improves the strain fixity but reduces the strain recovery due to the lubrication of the OOBA long chains. The successful combination of the liquid crystalline properties and multi-shape memory effect makes the PySMPU/OOBA complexes potentially applicable in smart optical devices, smart electronics and smart sensors.

**Keywords:** Supramolecular; shape memory; polyurethane; liquid crystal; crystallization;

## 1. Introduction

Recently, shape memory polymers (SMPs) have become increasingly important due to the growing number of applications in which they would be useful.<sup>1, 2</sup> In addition to the traditional dual-shape memory effect, the research of SMPs has developed multi-shape memory effects, which can fix two or more temporary shapes, recover from the first temporary shape to the other temporary shapes in sequence and finally return to its original shape.<sup>3-5</sup> The key factor to allow multi-shape-memory effects is the integration of two or more reversible phases into a polymer network.<sup>3-5</sup> One strategy is to incorporate several discrete thermal transitions into the material. Typical examples include macroscopic homogeneous polymers consisting of micro-separated distinctive phases, polymer composites, and macroscopic polymer bilayers.<sup>6</sup> An alternative strategy relies on a single broad thermal transition because a broad thermal transition can be thought to be composed of multiple distinct transitions.<sup>7</sup> For example, Xie and Li used a broad  $\alpha$ -transition to achieve a step-wise multi-shape memory and recovery.<sup>5, 8</sup> In this study, we present another strategy to achieve a multi-shape memory effect using supramolecular switches in supramolecular SMPs. The development of supramolecular multi-SMPs is believed to have more significant and broad-ranging technological impacts.

Supramolecular SMPs have been studied for many years.<sup>9-11</sup> The shape memory and recovery in common SMPs are usually designed based on a reversible phase transition, while supramolecular SMPs are synthesized using stimuli-sensitive supramolecular switches, such as hydrogen bonding,<sup>12, 13</sup> CD inclusion,<sup>14, 15</sup> or  $\pi$ - $\pi$  stacking. The reported supramolecular complex can be responsive not only to heat, pH and light but also to chemicals, redox reactions and glucose.<sup>16-18</sup> In recent years, supramolecular polymer complexes have even shown triple-shape memory functionalities. For example, an acrylic triple-SMP has been prepared using a glass transition and dissociation of self-complementary hydrogen bonding moieties.<sup>19</sup> Another triple-shape memory supramolecular composite was designed using intermolecular hydrogen bonding between a polymer and mesogenic units.<sup>20</sup> Although triple-shape memory functionality is achieved in this system, the polymer composite loses its supramolecular liquid crystalline properties. It is well known that supramolecular liquid crystalline polymers can provide an easy way to combine entropy-induced polymer elasticity and liquid crystalline ordering. Supramolecular liquid crystalline polymers have been widely studied in past decades.<sup>21, 22</sup> However, to our knowledge, there are few reports about

supramolecular liquid crystalline SMPs. In this study, we develop a novel supramolecular liquid crystalline complex that exhibits both a multi-shape memory effect and liquid crystalline properties.

In earlier studies, we successfully prepared liquid crystalline polyurethane composites with both liquid-crystalline properties and shape-memory properties by mixing 4-n-hexadecyloxybenzoic acid (HOBA) with shape-memory polyurethane based on an amorphous reversible phase<sup>23</sup> or a semi-crystalline reversible phase.<sup>24</sup> In addition to triple-shape memory effects and liquid crystalline properties, these liquid crystalline polyurethane composites also showed interesting self-healing properties.<sup>24</sup> Additionally, based on the investigations on supramolecular SMPs,<sup>25,26</sup> we developed one type of supramolecular liquid crystalline polyurethane complex that exhibited triple-shape functionality by incorporating HOBA with pyridine containing shape-memory polyurethane (PySMPU).<sup>27</sup> Different from the previous system, another type of liquid crystal mesogen, 4-n-octyldecyloxybenzoic acid (OOBA), was used as fillers in this study. The polymer matrix was also replaced with a modified PySMPU containing rigid, hard segments that reinforced the physical netpoints. Moreover, the present PySMPU/OOBA system has not only improved triple-shape memory properties, but also quadruple-shape memory behaviors. Thus, this new supramolecular liquid crystalline shape-memory polyurethane complex is expected to show more interesting liquid crystalline functionalities and multi-shape memory properties.

## 2. Experimentation

### 2.1 Materials

N,N-bis(2-hydroxyethyl)isonicotinamine (BINA) was purchased from the Jiaying Carry Bio-Chem Technology Co. Ltd. (Zhejiang, China). 1,6-hexamethylene diisocyanate (HDI), diphenylmethane diisocyanate (MDI), 1,4-butanediol (BDO) and dimethylformamide (DMF, HPLC) were purchased from Aladdin-reagent Co. Ltd. (Shanghai, China).

### 2.2 Synthesis of PySMPUs

In this study, PySMPUs were prepared using BINA, HDI, BDO and MDI in a DMF solution at a 1:1.05 molar ratio of OH to NCO based on the synthesis procedure described previously.<sup>18</sup> The synthesis routine is shown in Scheme 1. After dissolving the BINA powder in 10 mL of DMF, the reaction to prepare the prepolymer with BINA and HDI was performed at 80 °C for 2 h in a 500-mL flask filled with nitrogen and equipped with a mechanical stirrer, a thermal metre, and a condenser. A 0.02-wt% dibutyltin dilaurate catalyst was added to the reaction. Following the chain-extension

process with BDO and MDI for another 2 h, 10 mL of DMF was occasionally added to the reaction to control the viscosity of the solution. The reaction was maintained for 4 h to obtain a 10-wt% PySMPU/DMF solution.

### Scheme 1.

## 2.2 Preparation of PySMPU/OOBA Complexes

Based on the composition shown in Table 1, a certain quantity of OOBA (e.g., 1.02 g) was added to the PySMPU/DMF solution containing approximately 10.0 g of PySMPU resin. Under strong mechanical stirring, the PySMPU and OOBA were mixed for 2 h to obtain a homogenous solution-phase mixture. Finally, the final PySMPU/OOBA complex was obtained by casting the mixture onto a Teflon pan, which was incubated at 80°C for 24 h and further dried at 80°C under a vacuum of 0.1-0.2 kPa for 24 h. The samples were coded as PySMPU-#OOBA, where # represents the molar ratio of OOBA/BINA (e.g., sample PySMPU-0.4OOBA).

### Table 1.

## 2.3 Structural Characterization

FT-IR spectra were scanned from smooth polymer films with a thickness of 0.2 mm using a Nicolet 760 FT-IR spectrometer using the FT-IR attenuated total reflection (ATR) method. Ten scans at a resolution of 4 cm<sup>-1</sup> were averaged and stored as data files for further analysis.

Wide-angle X-ray diffraction (WAXD) measurements were obtained using a D8 Advance (Bruker, Germany) instrument with an X-ray wavelength of 0.154 nm at a scanning rate of 12°/min. Specimens that were 0.5 mm thick were prepared for these measurements.

DSC curves were obtained using a TA Q200 instrument with nitrogen as a purge gas. Indium and zinc standards were used for calibration, and the scanning rate used was 10°C/min.

Mesophases were identified, and the phase transition temperatures were determined using a Zeiss-Axioscope polarised optical microscope (POM) equipped with a Linkam-THMS-600 variable-temperature stage at a scan rate of 2°C/min. The samples were heated from 20°C to 160°C and cooled from 160°C to 20°C.

The dynamic mechanical properties of the samples were determined using a PerkinElmer DMA at 1 Hz with a heating rate of 3°C/min from -30 to 200°C. The specimens for DMA testing were prepared by casting a 0.5-mm-thick film with a width of 5 mm and a length of 25 mm.

The morphology of the samples was examined using scanning electron microscopy (SEM,

Hitachi, Japan) and high resolution transmission electron microscopy (HR-TEM, Tecnai G<sup>2</sup>F30, USA). Prior to SEM scanning, the samples were coated with a thin layer of gold.

## 2.4 Testing of Multi-Shape-Memory Behaviours

Thermally induced multi-shape memory behaviours were examined via thermo-mechanical analysis using a TA Instruments DMA800 with tension clamps in controlled-force mode, according to the procedure described in the literature.<sup>2, 5, 23, 24, 27</sup> All samples were dried at 100°C *in vacuo* for 24 h and cut into rectangular pieces of 10 mm × 2.0 mm × 0.5 mm. The detailed test setup for the triple- and quadruple-shape-memory cycles are provided below.<sup>28</sup>

a) For the triple-shape-memory cycles: (1) the samples were heated to ca. 100°C and equilibrated for 20 min; (2) uniaxial stretching was applied by ramping the force from 0.001 N to 1 N at a rate of 0.25N/min; the samples were then allowed to equilibrate for 3 min; (3) the strain was then fixed via rapid cooling to 70°C at a cooling rate (*q*) of -10°C/min, followed by equilibration for 10 min; (4) further fixing of the strain occurred via rapid cooling to 20°C with *q*=-10°C/min, followed by equilibration for 10 min; (5) the external force was then unloaded to 0 N at a rate of 0.25 N/min; (6) the samples were then reheated to 70°C at a rate of 4°C/min, followed by equilibration for 40 min; and (7) lastly, the samples were reheated again to ca. 100°C at a rate of 4°C/min and allowed to equilibrate for 40 min.

b) For the quadruple-shape-memory cycles: (1) the samples were first heated to 110°C and allowed to equilibrate for 20 min; (2) the samples then underwent uniaxial stretching by ramping the force from 0.001 N to 1 N at a rate of 0.25 N/min, followed by equilibration for 3 min; (3) the strain was then fixed via rapid cooling to 90°C with *q*=-10°C/min, followed by equilibration for 10 min; (4) further fixing of the strain occurred via rapid cooling to 70°C with *q*=-10°C/min, followed by equilibration for 10 min; (5) again, the strain was fixed further via rapid cooling to 0°C with *q*=-10°C/min, followed by equilibration for 10 min; (6) the external force was then unloaded to 0 N at a rate of 0.25 N/min; (7) the samples were then reheated to 70°C at a rate of 4°C/min, followed by equilibration for 40 min; (8) further reheating then occurred up to 90°C at a rate of 4°C/min, followed by equilibration for 40 min; and (9) lastly, the samples underwent reheating to 110°C at a rate of 4°C/min and were then allowed to equilibrate for 40 min.

## 3. Results and Discussion

### 3.1 Structure analysis

**Figure 1.**

The molecular structures of the PySMPU/OOBA complex, pure PySMPU and OOBA were investigated with FT-IR (see **Figure 1**). The N–H stretching vibration detected at approximately 3315–3320  $\text{cm}^{-1}$  shows the formation of urethane groups in both the pure PySMPU and the PySMPU/OOBA complex. Compared with the pure PySMPU, the PySMPU/OOBA complex (e.g., sample PySMPU-0.2OOBA) exhibits new frequencies at approximately 1256  $\text{cm}^{-1}$  and 1169  $\text{cm}^{-1}$ , which were also observed in pure OOBA (see **Figure 1a**). The frequency at approximately 1169  $\text{cm}^{-1}$  likely resulted from the C–O stretching vibration of OOBA; this suggests that the OOBA has been successfully incorporated into the PySMPU, forming a PySMPU/OOBA complex. Additionally, it was reported that the frequencies at 1600, 1464, 1411, and 1136  $\text{cm}^{-1}$  resulted from the stretching vibration of the hydrogen-bonded pyridine ring. When OOBA is incorporated into PySMPU, the peak intensity at 1624  $\text{cm}^{-1}$  weakens, and the frequency shifts from 1600  $\text{cm}^{-1}$  to 1604  $\text{cm}^{-1}$ ; this result implies that the stretching vibration at the position of C=O next to the pyridine ring is affected by the incorporated OOBA. Additionally, the stretching frequencies at the pyridine ring (e.g., 1600, 1464, 1411 and 1136  $\text{cm}^{-1}$ ) all shift to higher frequencies (e.g., 1604, 1469, 1413 and 1139  $\text{cm}^{-1}$ ) in sample PySMPU-0.2OOBA (see **Figure 1a**). These results also suggest that the stretching vibration of the pyridine ring is limited by the OOBA. It is thus confirmed that OOBA is connected to PySMPU as a side chain *via* strong hydrogen bonding in the PySMPU/OOBA complex. This result can also be verified from the FT-IR spectra of PySMPU/OOBA complexes with various OOBA content (See **Figure 1b**). The increase in the OOBA content in the samples is confirmed from the increase in the peak density at 1256  $\text{cm}^{-1}$ , which is the stretching vibration frequency of C–O in OOBA.

The supramolecular structure of the PySMPU/OOBA complex can be further confirmed by WAXD, as shown in Figure 2. Pure PySMPU has an amorphous phase, while the pure OOBA forms a crystal, as indicated by its many crystalline peaks (see **Figure 2a**). In the PySMPU/OOBA complexes (e.g., the PySMPU-1.0OOBA samples), nearly all of the crystalline peaks of OOBA could be detected. The peak intensity also increases with increasing OOBA content (see **Figure 2b**). In a previous report, Chen et al. demonstrated that the liquid crystalline mesophase was lost when LC mesogens containing pyridine moieties were attached to the SMPU-containing carboxyl groups *via* hydrogen bonding between the pyridines and the COOH groups.<sup>23</sup> However, in this

PySMPU/OOBA complex, the pendant pyridine rings connect to the mesogens as side chains. As a result, the intrinsic liquid crystalline properties of OOBA are maintained. This study also suggests that better liquid crystalline properties can be achieved by adding large amounts of OOBA mesogens.

Based on the above analysis, the possible supramolecular structure of the PySMPU/OOBA complex is proposed in Scheme 2. In this study, a liquid crystal mesogen (i.e., OOBA) was used because OOBA has been reported to show several types of phase transitions, including a crystal-liquid crystalline phase transition and a liquid crystalline-isotropic phase transition.<sup>29</sup> Crystals of OOBA were also found to have three crystalline forms.<sup>30</sup> In this PySMPU/OOBA complex, different from the previously reported HOBA/PySMPU complex,<sup>27</sup> the polymer backbone of the present PySMPU was composed of a HDI-BINA segment and a MDI-BDO segment. The pendant pyridine rings of a BINA unit were used as H-acceptors, while MDI-BDO was used to reinforce the polymer backbone as hard segment fillers. Thus, similar to the HOBA/PySMPU system,<sup>27</sup> strong hydrogen bonds could be formed between the pyridine rings and the carboxyl groups of OOBA in the PySMPU/OOBA system. The MDI-BDO rigid hard segment would thus provide more stable physical netpoints to the polymer backbone (Scheme 2).

### Figure 2

### Scheme 2.

## 3.2 Thermal properties

The thermal properties and phase transitions of the PySMPU/OOBA complex were investigated systematically using DSC. The second DSC heating curves demonstrate that pure PySMPU has only one glass transition at 30.5°C. Pure OOBA shows three large endothermic peaks (See Figure 3a); among them, the first two peaks at 78°C and 102°C can be attributed to the crystal melting transitions of the  $\alpha$  and  $\beta$  crystalline phases, respectively, while the third peak likely indicates a nematic-isotropic phase transition. These phase transitions are verified by the following POM investigations. When the OOBA mesogen is connected to the PySMPU backbone via hydrogen bonding, the glass transition of the PySMPU and the two crystal melting transitions were all located on the second DSC heating curve of the PySMPU/OOBA complex (see Figure 3a). A new weak phase transition that may be attributed to the smectic-nematic phase transition

occurs at 118°C because the smectic liquid crystalline of OOBA was reported at this temperature region.<sup>29</sup> On the cooling curves, the glass transition was also determined to be near 30°C; crystallization peak occurred at 52-54°C (see **Figure 3b**). As the OOBA content increases, the crystallization peak grows significantly. In the samples with higher OOBA contents (e.g., PySMPU-1.0OOBA), in addition to the second crystallization peak at 94°C, the phase transition from the nematic-to-smectic phase transition was also determined to occur from 102°C to 115°C (see **Figure 3(b)**). It is thus confirmed that both the crystallization behaviour and the liquid crystalline properties of OOBA were maintained in the PySMPU/OOBA complex.

Additionally, the first DSC heating curves demonstrate that the glass transition temperature ( $T_g$ ) shifts to a higher temperature as the OOBA content increases (see **Figure 3c**). This result implies that the OOBA reinforces the PySMPU polymer matrix, serving as crystal fillers. The increased peak density also suggests a higher crystallinity in the PySMPU/OOBA complex with higher OOBA content. However, on the second heating curves, the glass transition process appears to become more complex because the OOBA serves as crystal fillers and as a plasticizer. When no crystals are formed, the  $T_g$  shifts to a lower temperature due to the lubrication functionality (e.g., sample PySMPU-0.2OOBA). In the sample containing a large fraction of OOBA crystals, the  $T_g$  shifts to a higher temperature due to reinforcement (e.g., sample PySMPU-0.6OOBA), while the OOBA molecules also lubricate the polymer chains, reducing the  $T_g$  (e.g., sample PySMPU-1.0OOBA, see **Figure 3d**). These DSC heating curves also demonstrate that the PySMPU/OOBA complex is formed gradually upon cooling; whereas the hydrogen bonding is destroyed easily and the complex might be decomposed during crystallization. After cooling from high temperature, hydrogen bonding is formed gradually, and the strength gets stronger at lower temperature. Due to the limitation of polymer matrix, the incorporated OOBA molecules could not form crystals within a short time, but need a long crystallization time. Therefore,  $T_m$  is detected on the first heating curves in all samples (see **Figure 3c**); whereas no  $T_m$  is detected on the second heating curves in sample PySMPU-0.2OOBA; and thermal-induced recrystallization occurs in other samples (see **Figure 3d**). Compared with the first heating curves, the first crystal melting transition of OOBA in the complex is shown to overlap with the second recrystallization transition in the second heating process. Additionally, the second DSC heating curves also demonstrate that the smectic-nematic phase transition increases in magnitude, while the nematic-isotropic phase

transition tends to decrease in magnitude (see **Figure 3d**). A possible reason for these results is that the movement of the OOBA molecules is influenced by the PySMPU polymer matrix; thus, the nematic liquid crystalline phase might be limited, while smectic liquid crystalline phase might be promoted because the molecular structure of the smectic liquid crystalline phase is near that of the crystalline phase.

### Figure 3.

The influence of the heat treatment on the thermal-properties of the PySMPU/OOBA complexes were also investigated with DSC by heating samples up to 100, 120, 140 and 160°C, respectively (see **Figure 4**). When sample PySMPU-0.6OOBA was treated at 100°C, the glass transition of PySMPU, the  $\alpha$  crystal melting transition and the  $\beta$  crystal melting transition were all determined based on the second heating curves. The  $\alpha$  crystal melting transition was found to weaken as the heat treatment temperature increases from 100 to 140°C and finally disappear at 160°C (see **Figure 4a**). A possible reason for this result is that higher treatment temperatures promote the movement of polymer chains, destroying the OOBA crystallizations; this also affects the formation of the liquid crystalline phase. As the temperature increases, the nematic-isotropic phase transition weakens, while the smectic-nematic phase transition strengthens on the second DSC heating curves. This hypothesis was also confirmed on the cooling curves. Two crystallization peaks were detected when the heat treatment temperature was lower than 100°C, while the smectic-crystal phase transition was detected on the cooling curves after heat treatment above 120°C (see **Figure 4b**). It is thus confirmed again that multiple distinct transitions were combined in the PySMPU/OOBA complex, providing the structural conditions to achieve multi-shape memory effects. The liquid crystalline properties could also be adjusted by the heat treatment applied and by the PySMPU polymer matrix used.

### Figure 4.

#### 3.3 Dynamic mechanical properties

Other important conditions for the multi-shape memory effect are the temperature-dependent visco-elastic properties, which are primarily embodied in the dynamical mechanical properties.<sup>29</sup> The DMA curves of PySMPU/OOBA complexes show that the PySMPU/OOBA complexes and pure PySMPU exhibit similar trends in their storage modulus below 90°C (see **Figure 5A**). The samples have a large glassy modulus ( $E_g'$ ) below 0°C, while the storage modulus decreases

gradually during the glass transition process. When OOBA is connected to the PySMPU, the glassy modulus also decreases significantly in samples PySMPU-0.6OOBA, PySMPU-0.8OOBA and PySMPU-1.0OOBA. A possible reason for this is that the original intermolecular hydrogen bonding of PySMPU was replaced with new hydrogen bonds between the OOBA with pyridine rings in the PySMPU/OOBA complex. This provides more proof of the formation of a supramolecular liquid crystalline complex. As the temperature increases, the modulus changes significantly from 47°C to 100°C. The pure PySMPU and the PySMPU/OOBA complexes with lower OOBA contents (e.g., samples PySMPU-0.2OOBA, PySMPU-0.4OOBA) show stable rubber modulus, while a second modulus change occurs above 110°C in the samples with higher OOBA contents (e.g., samples PySMPU-0.8OOBA, PySMPU-1.0OOBA). The decrease in the modulus in the first stage likely occurred due to the glass transition of PySMPU, while the second decrease in the modulus likely occurred due to the crystal melting transition of the OOBA mesogen because the central temperature for the second decrease in the modulus exactly corresponds to the  $T_m$  of OOBA, as discussed regarding the DSC curves. Additionally, the DMA curves demonstrate that the rubber modulus between 90 and 110°C in the PySMPU/OOBA complex tends to be higher than that of pure PySMPU; this result suggests that the OOBA crystals reinforce the rubber modulus acting as crystal fillers in the rubber state. It is thus confirmed again that a phase separation structure exists in the PySMPU/OOBA complex. In addition to the glass transition of the PySMPU matrix, the OOBA crystalline phase might provide another reversible phase for the shape memory effect. This result is consistent with the DSC results. Additionally, the  $\tan(\delta)$  curves demonstrate that the PySMPU matrix exhibits a broad glass transition, ranging from 50 to 120°C (see **Figure 5B**). This broad glass transition also provides multiple distinct transitions to achieve multi-shape memory effects. Finally, the loss modulus curves provide other information regarding the intermolecular interaction of the PySMPU/OOBA complex. The maximum loss modulus occurs during the glass transition process in all samples because significant movement of the polymer chain occurs during the glass transition process (see **Figure 5C**). Particularly, the pure PySMPU shows the largest loss modulus within all temperature ranges due to the strong intermolecular hydrogen bonds present among the urethane groups and between the pyridine ring and the urethane group. When the OOBA is mixed with the PySMPU, intermolecular hydrogen bonding is destroyed, and OOBA also serves as the plasticizer due to its long chains. Therefore, the maximum loss modulus decreases as the OOBA content

increases (see **Figure 5D**).

### Figure 5.

#### 3.4 Morphology

The surface morphology and broken surface of the PySMPU/OOBA complexes is investigated with SEM. Surface SEM images demonstrate that the pure PySMPU has a smooth surface without any holes (see **Fig. 6a**), while the surface of the sample becomes rough in the PySMPU/OOBA complex (see **Figure 6b**). As the OOBA content increases, an increasing number of cracks are observed in samples SMPU-0.6HOBA, SMPU-0.8HOBA and SMPU-1.0HOBA. Additionally, SEM images of the broken surface demonstrate that the PySMPU/OOBA complexes have a phase separated structure (see **Figure 6c-d**). HR-TEM images further show that the polymer matrix is an amorphous phase while another phase is crystalline phase of OOBA (see **Figure 6e-f**). This conclusion could be verified from the bright image and the corresponded POM image (see **supporting information Figure SI 1**). SEM/EDS elemental spectrum further confirm that the elemental ratio of C/O in the crystalline region is much higher than that in the amorphous phase, though the N elements are overlapped by C peak (see **supporting information Figure SI 2**). It is thus confirmed that the crystals are resulted from the OOBA while the amorphous phase is ascribed to PySMPU matrix. This result is very consistent with the DSC analysis. A similar observation is also reported in the HOBA/PySMPU complex<sup>27</sup>. These OOBA crystals thus endow the PySMPU/OOBA complex with liquid crystalline properties.

### Figure 6

#### 3.5 Liquid crystalline properties

### Figure 7.

The liquid crystalline properties and phase transition behaviours of the PySMPU/OOBA complex were investigated by POM. In the literature,<sup>30</sup> it was reported that OOBA forms three crystalline forms, followed by smectic and nematic liquid crystalline phases upon heating.<sup>29</sup> These phase transitions of pure OOBA are confirmed by POM. At 40°C, OOBA forms a stable crystalline phase (crystal  $\alpha$ , see **Figure 7a**). When the temperature increases to 80°C, the crystal  $\alpha$  changes to another crystalline phase (crystal  $\beta$ , see **Figure 7b**). As the temperature increases continuously, the crystal  $\beta$  changes to a third crystalline phase (crystal  $\gamma$ ), which overlaps the phase transition from crystal  $\gamma$  phase to the smectic phase at 110°C (see **Figure 7c**). Finally, the smectic phase transitions

to the nematic liquid crystalline phase at 148°C (see **Figure 7d**). When OOBA is mixed with PySMPU in the PySMPU/OOBA complex, a continuous OOBA phase tends to disperse into the isolated OOBA phase in a polymer matrix when the OOBA content is low (e.g., samples PySMPU-0.2OOBA, PySMPU-0.4OOBA and PySMPU-0.6OOBA, see **Figures 7m-x**). The size of the isolated OOBA phase increases as the OOBA content increase (see **Figure 7m, q, u**). Thus, a two-phase separated structure was also found in the POM image. The black phase is the PySMPU phase, and the bright phase is the OOBA crystalline phase (see **Figure 7m**). When the OOBA content is higher, the OOBA phase could also form a continuous OOBA coating on the surface of the polymer complex (see **Figure 7e-l**). The crystalline behaviours of the OOBA are maintained in all of the PySMPU/OOBA complexes. Figure 7 shows that all of the PySMPU/OOBA complexes exhibit a  $\alpha$  crystalline phase at 40°C that changes to a  $\beta$  crystalline phase at 80°C. Similar to pure OOBA, the PySMPU/OOBA complex tends to show an overlapped texture of a  $\gamma$  crystalline phase and a smectic liquid crystalline phase at 110°C (e.g., sample PySMPU-0.6OOBA). At 148°C, the schlieren brush texture of the nematic phase was detected in samples PySMPU-0.8OOBA (see **Figure 7l**) and PySMPU-1.0OOBA (see **Figure 7h**). When the OOBA content is low (e.g., samples PySMPU-0.2OOBA, PySMPU-0.4OOBA), the POM did not show the clear textures typical of crystalline and liquid crystalline phases; however, the phase transitions could be distinguished by changing the light polarization (see **Figures 7u, v, w, x**).

### Figure 8.

The phase transition of the PySMPU/OOBA complex was also investigated via temperature-dependent WAXD. The WAXD spectra at various temperatures show that the crystalline peaks insignificantly change in samples PySMPU-0.4OOBA and PySMPU-0.8OOBA below 50°C (see **Figure 8**). These crystalline peaks indicate the presence of the  $\alpha$  crystalline phase, as discussed in DSC. When the temperature is increased to 80°C, the crystalline peaks change significantly, suggesting a phase transition from the  $\alpha$  crystalline phase to the  $\beta$  crystalline phase. Finally, no crystalline peaks are detected above 120°C, suggesting that crystal melting transitions have occurred completely. It is thus confirmed again that the PySMPU/OOBA enters the liquid crystalline phase above 120°C. Compared with pure OOBA, the PySMPU/OOBA complexes maintain the intrinsic liquid-crystalline properties of OOBA and form a stable film for various applications as polymeric film materials.

### 3.6 Multi-shape memory properties

Figure 9 shows the strain-stress-temperature-time curve of the PySMPU/OOBA complexes developed in this study, showing the triple-shape memory effects of these materials. Figure 9A shows that PySMPU-0.2OOBA could be deformed by a strain of approximately 100% when the sample was heated to 100°C, and nearly all of the deformations were fixed after cooling below 0°C. More than 90% strain recovery is shown to occur during reheating to the deformation temperature; this is typical triple-shape memory behaviour. The other PySMPU/OOBA complexes with different OOBA contents also show similar triple-shape memory behaviours (see **Figures 9B, C, D, E**). Overall, the strain fixity in the first stage is generally lower than that in the second stage due to the higher fixing temperature and consequently higher chain mobility in the first stage. The strain fixities in both the first and the second stages increase with increasing OOBA content because the crystallization increases as the OOBA content increases, as discussed in the DSC analysis. Similarly, the strain recovery in the first stage is considerably higher than that in the second stage. Increasing OOBA content thus leads to a decrease in shape recovery, despite good shape fixities in all samples (see **Figures 9B-E**). One reason for these results is that OOBA disturbs the hydrogen-bonded physical cross-linking of PySMPU, which serves as physical netpoints for shape recovery. This hypothesis is supported by the decreased H-bonding between urethane groups with increased OOBA content in the FT-IR analysis above. Another possible reason for these results is that the lubrications of OOBA promote phase mixing, destroying the elasticity of the polymer chain because the DMA showed increased phase mixing with increased OOBA content. This hypothesis is also supported by the stress relaxation tests. During the first and second strain recovery processes, the stresses resulting from the strain recovery both reduce as the OOBA content increases. The resulting recovery force in the first stage is considerably higher due to the lower recovery temperature (see **Figure 10**). Finally, the PySMPU/OOBA complex was found to have good quadruple-shape memory effects. Figure 11 shows that the quadruple-shape memory behaviours of sample PySMPU-0.2OOBA are equally good when fixing the three temporary shapes at 90, 70, and 0°C, and recovered at 70, 90, and 110°C, respectively. It is thus confirmed that the PySMPU/OOBA complex shows multi-shape memory effects. These observations make PySMPU/OOBA complexes good candidates for potential applications in smart optical devices and sensors, which will be explored in future studies.

**Figure 9.**

**Figure 10.**

**Figure 11.**

#### **4. Conclusions**

This paper describes a supramolecular liquid crystalline shape-memory polyurethane complex that exhibits both liquid crystalline properties and multi-shape memory properties by incorporating OOBA into PySMPUs. Molecular analyses show that the OOBA was connected to the PySMPU via strong hydrogen bonds to form a PySMPU/OOBA complex. The results demonstrate that the PySMPU/OOBA complex not only maintains the intrinsic crystallization and liquid-crystalline properties of OOBA but also combines the multi-shape memory properties of PySMPU and forms a stable polymeric film for various shape memory applications. Shape memory investigations demonstrate that the PySMPU/OOBA complexes have good multi-shape memory effects, including triple- and quadruple-shape memory behaviours. In the triple-shape memory behaviour of the material, the strain fixity at the first stage is lower than that at the second stage, while the strain recovery at the first stage is considerably higher than that at the second stage. Overall, increasing the OOBA content improves the strain fixity due to the increased crystallization but reduces the strain recovery by lubricating the OOBA long chains. The successful combination of liquid crystalline properties and the multi-shape memory effect gives the PySMPU/OOBA complexes significant potential applications in smart optical devices, smart electronics and smart sensors.

#### **Acknowledgements**

This work was financially supported by the National Natural Science Foundation of China (grant No. 21104045); the Special Research Foundation of Shenzhen Overseas High-level Talents for Innovation and Entrepreneurship (Grant No. KQCX20120807153115869), the Nanshan District Key Lab for Biopolymers and Safety Evaluation (No. KC2014ZDZJ0001A), the Natural Science Foundation of Guangdong (Grant No. S2013010013056 and 2014A030313559), the Science and Technology Project of Shenzhen City (Grant No. JCYJ20140828163633993), and the cultivate special funds of Guangdong province college students' scientific and technological innovation (special funds for the climbing program).

## References

1. J. Hu and S. Chen, *Journal of Materials Chemistry*, 2010, **20**, 3346-3355.
2. S. Chen, F. Mo, Y. Yang, F. J. Stadler, S. Chen, H. Yang and Z. Ge, *Journal of Materials Chemistry A* 2015, **3**, 2924-2933.
3. L. Sun and W. M. Huang, *Soft Matter*, 2013, **6**, 4403-4406.
4. K. Yu, T. Xie, J. Leng, Y. Ding and H. J. Qi, *Soft Matter*, 2012, **8**, 5687-5695.
5. T. Xie, *Nature*, 2010, **464**, 267-270.
6. G. J. Berg, M. K. McBride, C. Wang and C. N. Bowman, *Polymer*, 2014, **55**, 5849-5872.
7. H. Meng, H. Mohamadian, M. Stubblefield, D. Jerro, S. Ibekwe, S.-S. Pang and G. Li, *Smart Materials and Structures*, 2013, **22**.
8. J. J. Li and T. Xie, *Macromolecules*, 2011, **44**, 175-180.
9. S. Zhang, Z. J. Yu, T. Govender, H. Y. Luo and B. J. Li, *Polymer*, 2008, **49**, 3205-3210.
10. S. J. Chen, *PhD thesis of The Hong Kong Polytechnic University.*, 2010.
11. S. J. Chen, J. L. Hu, S. G. Chen and C. L. Zhang, *Smart Materials & Structures*, 2011, **20**, -.
12. M. Guo, L. M. Pitet, H. M. Wyss, M. Vos, P. Y. W. Dankers and E. W. Meijer, *Journal of the American Chemical Society*, 2014, **136**, 6969-6977.
13. M. Wei, M. Zhan, D. Yu, H. Xie, M. He, K. Yang and Y. Wang, *Acs Applied Materials & Interfaces*, 2015, **7**, 2585-2596.
14. M. M. Fan, Z. J. Yu, H. Y. Luo, Z. Sheng and B. J. Li, *Macromolecular Rapid Communications*, 2009, **30**, 897-903.
15. H. Y. Luo, Y. Liu, Z. J. Yu, S. Zhang and B. J. Li, *Biomacromolecules*, 2008, **9**, 2573-2577.
16. Z.-Q. Dong, Y. Cao, Q.-J. Yuan, Y.-F. Wang, J.-H. Li, B.-J. Li and S. Zhang, *Macromolecular Rapid Communications*, 2013, **34**, 867-872.
17. J. R. Kumpfer and S. J. Rowan, *Journal of the American Chemical Society*, **133**, 12866-12874.
18. S. Chen, J. Hu, C.-w. M. Yuen and L. Chan, *Materials Letters*, 2009, **63**, 1462-1464.
19. T. Ware, K. Hearon, A. Lonneck, K. L. Wooley, D. J. Maitland and W. Voit, *Macromolecules*, **45**, 1062-1069.
20. H. Chen, Y. Liu, T. Gong, L. Wang, K. Zhao and S. Zhou, *RSC Advances*, 2013, **3**, 7048-7056.
21. M. Goel and M. Jayakannan, *Journal of Physical Chemistry B*, 2010, **114**, 12508-12519.
22. X. H. Cheng, J. Jin, Q. A. Li and X. Dong, *Chinese Journal of Chemistry*, 2010, **28**, 1957-1962.

23. S. Chen, H. Yuan, Z. Ge, S. Chen, H. Zhuo and J. Liu, *Journal of Materials Chemistry C*, 2014, **2**, 1041-1049.
24. S. Chen, H. Yuan, H. Zhuo, S. Chen, H. Yang, Z. Ge and J. Liu, *Journal of Materials Chemistry C*, 2014, **2**, 4203-4212.
25. S. J. Chen, J. L. Hu, H. T. Zhuo and S. G. Chen, *Journal of Materials Science*, 2011, **46**, 5294-5304.
26. S. J. Chen, J. L. Hu, S. G. Chen and C. L. Zhang, *Smart Materials & Structures*, 2011, **20**, 06500301-06500309.
27. S. Chen, H. Yuan, S. Chen, H. Yang, Z. Ge, H. Zhuo and J. Liu, *Journal of Materials Chemistry A*, 2014, **2**, 10169-10181.
28. R. Dolog and R. A. Weiss, *Macromolecules*, 2013, **46**, 7845-7852.
29. A. J. Herbert, *Transactions of the Faraday Society*, 1967, **63**, 555-&.
30. M. Ikeda and T. Hatakeyama, *Molecular Crystals and Liquid Crystals*, 1976, **33**, 201-212.

**New insights into multi-shape memory behaviours and liquid crystalline properties of supramolecular polyurethane complexes based on pyridine-containing polyurethane and 4-n-Octyldecyloxybenzoic acid**

Shaojun Chen<sup>1</sup>, Funian Mo<sup>1</sup>, Shiguo Chen<sup>1</sup>, Zaochuan Ge<sup>1</sup>, Haipeng Yang<sup>1</sup>, Jiandong Zuo<sup>1</sup>, Xinke Liu<sup>1\*</sup>, Haitao Zhuo<sup>2\*</sup>,

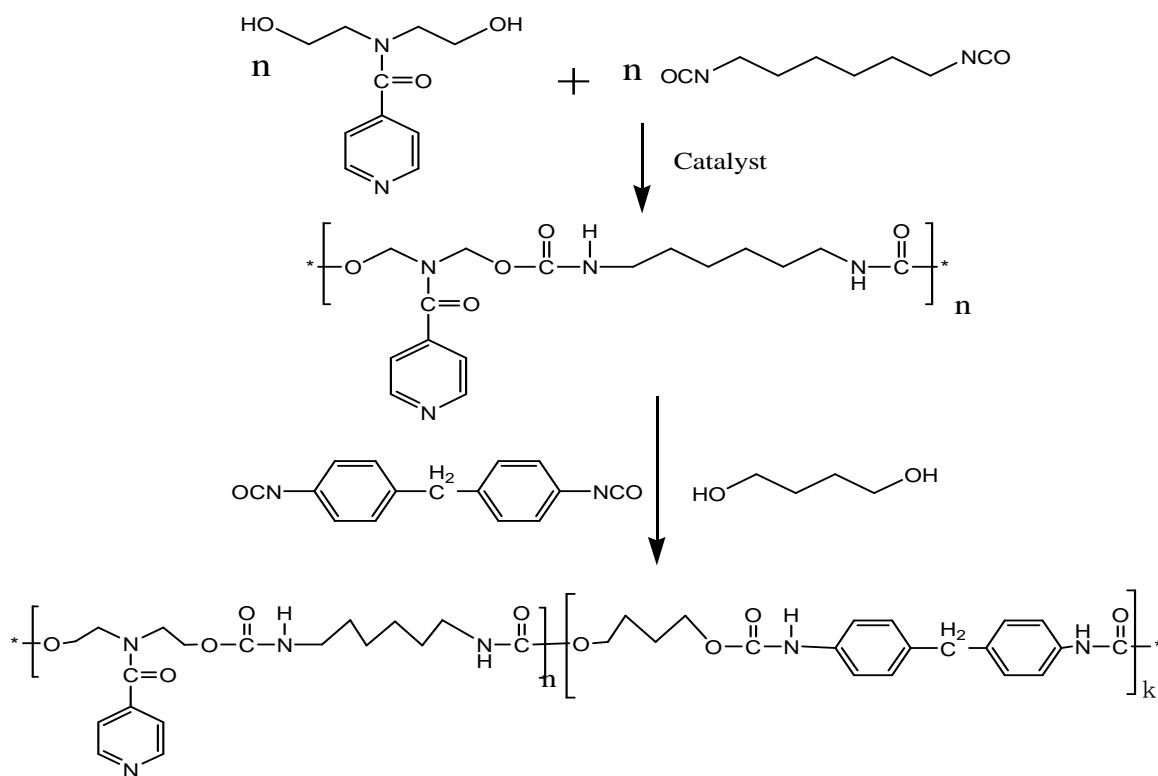
<sup>1</sup>Shenzhen Key Laboratory of Special Functional Materials, Nanshan District Key Lab for Biopolymers and Safety Evaluation, College of Materials Science and Engineering, Shenzhen University, Shenzhen, 518060, China. <sup>2</sup> College of Chemistry and Chemical Engineering, Shenzhen University, Shenzhen, 518060, China.

Corresponding authors: College of Materials Science and Engineering, Shenzhen University, Shenzhen, 518060, China. E-mail: X.K. Liu [xkliu@szu.edu.cn](mailto:xkliu@szu.edu.cn); H.T.Zhuo, [haitaozhuo@163.com](mailto:haitaozhuo@163.com)

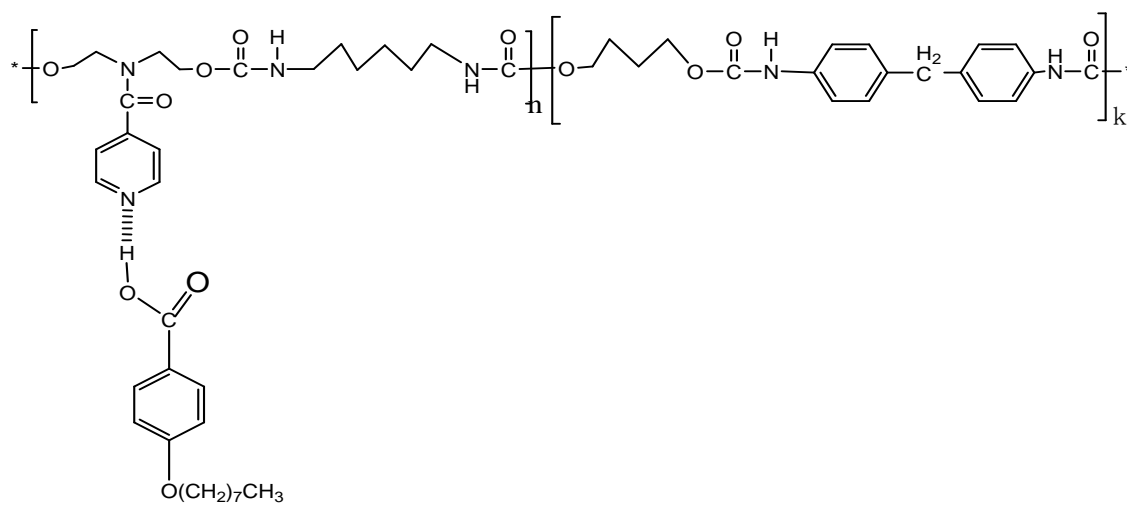
**Table, Schemes and Figures**

**Table1.Composition of PySMPU/OOBA complexes**

Sample	PySMPU(g)	OOBA(g)	OOBA content (wt%)	Molar ratio of OOBA/BINA
PySMPU	10.0	--	--	--
PySMPU-0.2 OOBA	10.0	1.02	9.3	0.2
PySMPU -0.4 OOBA	10.0	2.26	18.4	0.4
PySMPU -0.6 OOBA	10.0	3.83	27.7	0.6
PySMPU -0.8 OOBA	10.0	5.85	36.9	0.8
PySMPU -1.0 OOBA	10.0	8.56	46.1	1.0



Scheme 1. Synthesis routine of PySMPU



Scheme 2. Supramolecular molecular structure of PySMPU/OOBA complex

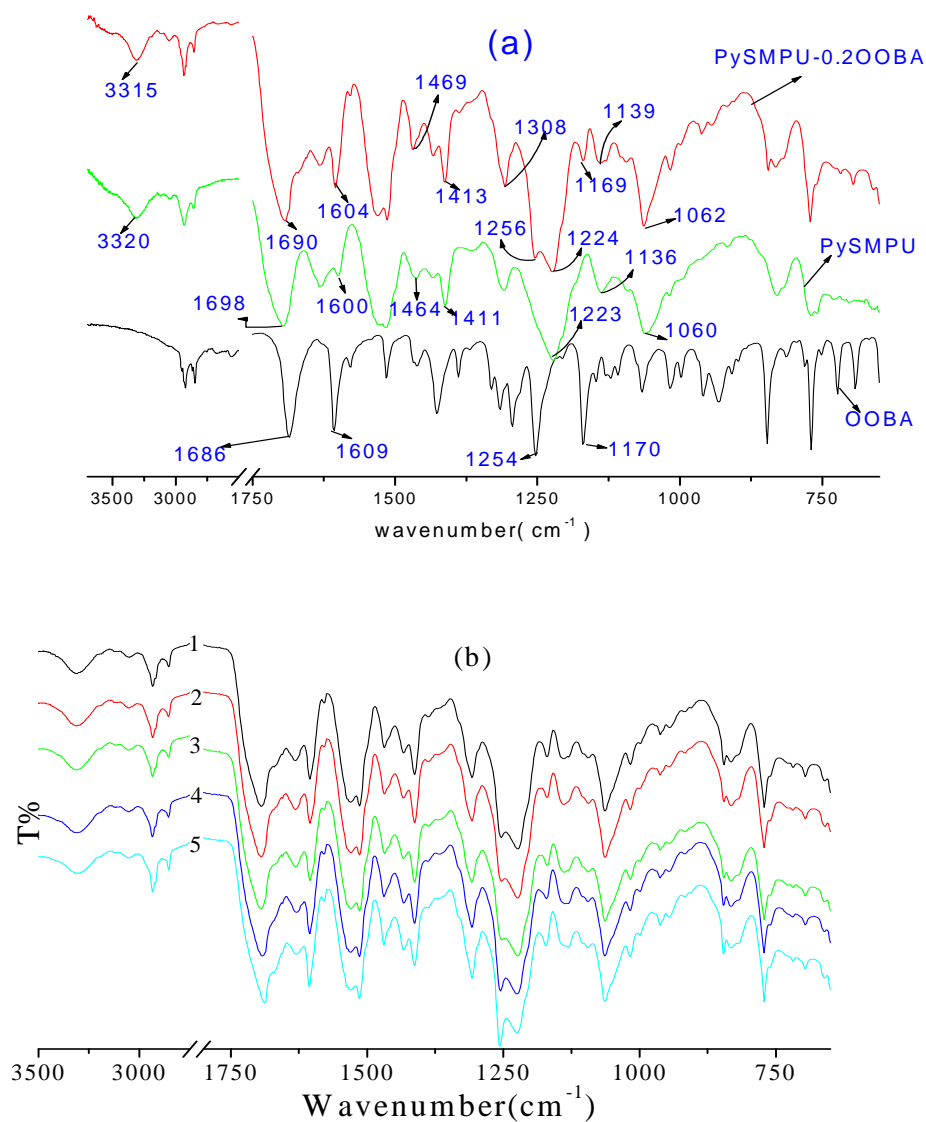


Figure 1. FTIR spectra of ((a) PySMPU-0.2OOBA, pure PySMPU and OOBA; (b) PySMPU with various OOBA (1- PySMPU-0.2OOBA; 2- PySMPU-0.4OOBA; 3- PySMPU-0.6OOBA; 4- PySMPU-0.8OOBA; 5- PySMPU-1.0OOBA)

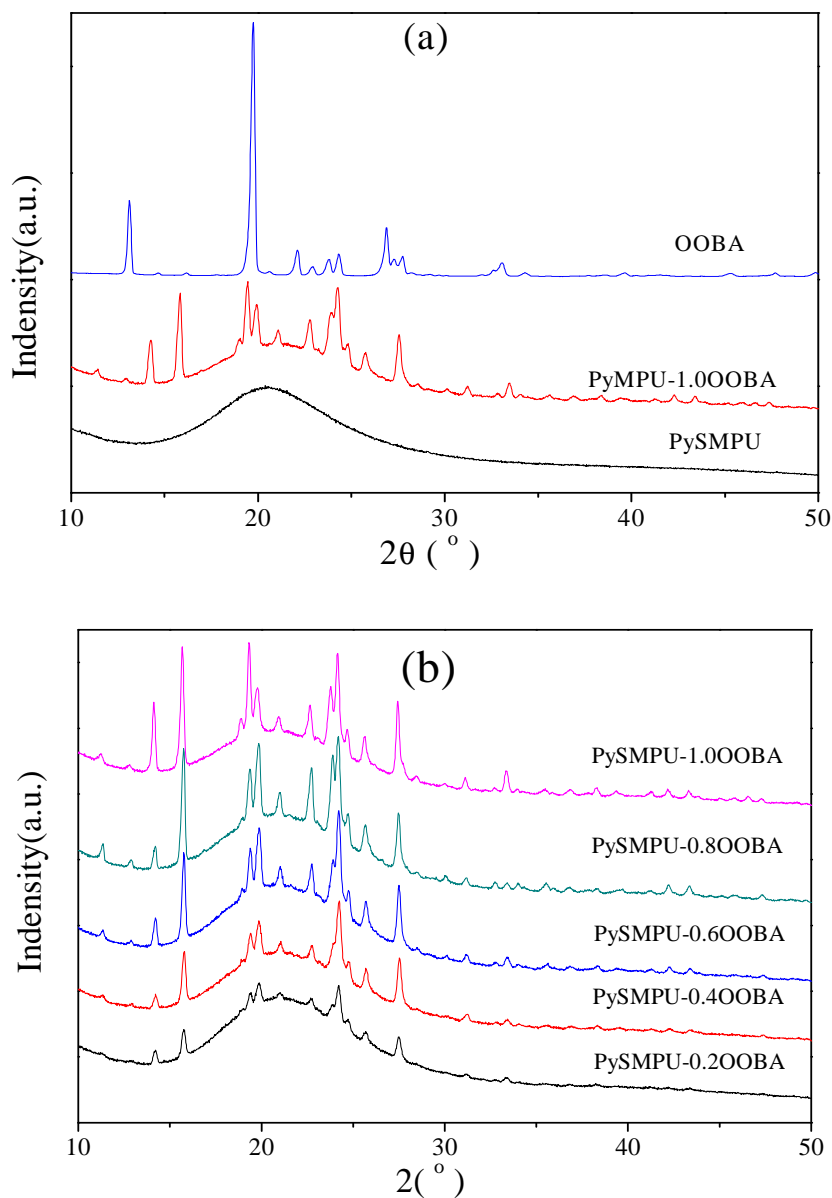


Figure 2. WAXD spectra of ((a) PySMPU/OOBA as compared with pure PySMPU and OOBA; (b) PySMPU/OOBA with various OOBA content: PySMPU-0.2OOBA, PySMPU-0.4OOBA, PySMPU-0.6OOBA, PySMPU-0.8OOBA, PySMPU-1.0OOBA)

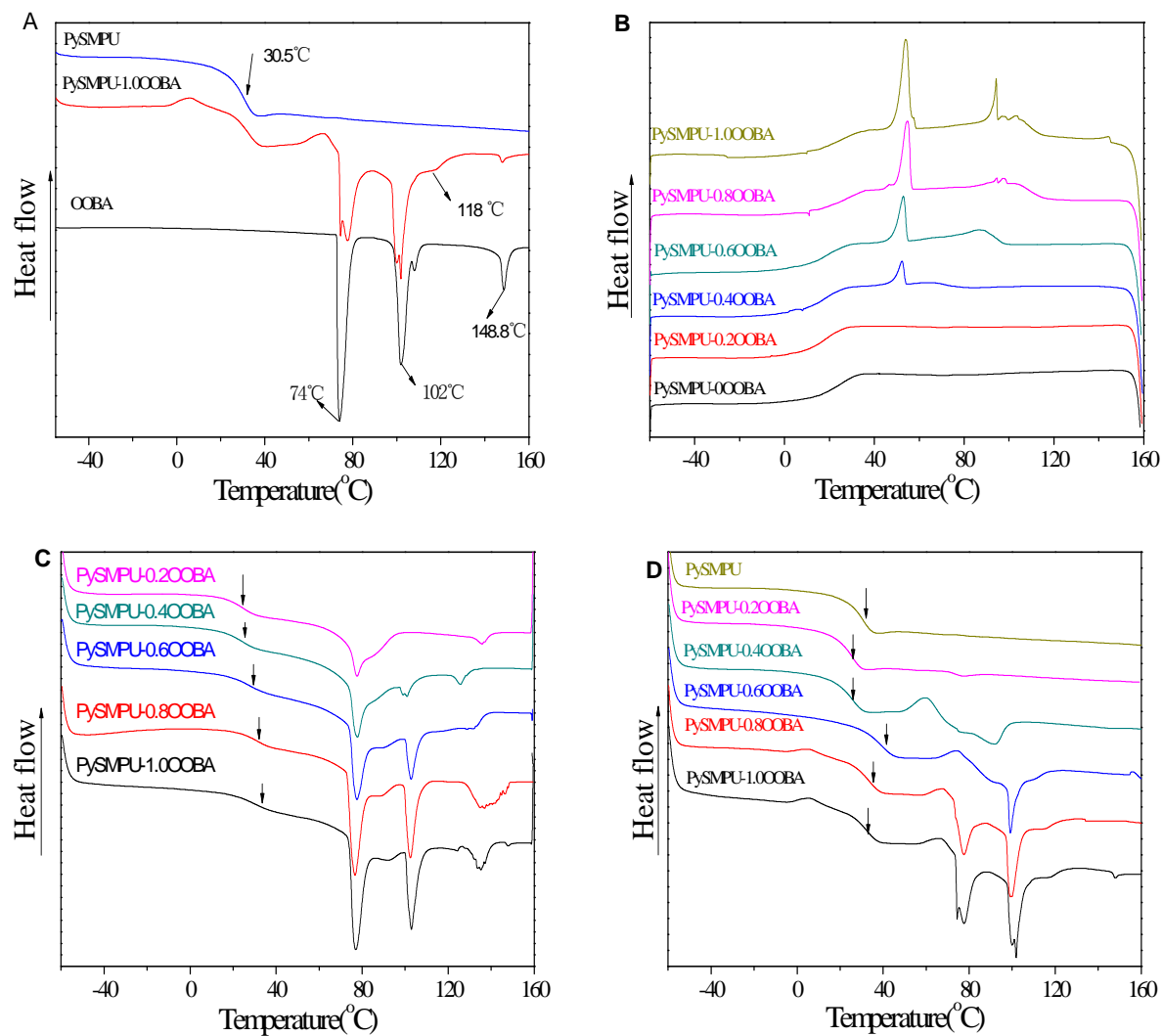


Figure 3. The DSC curves of samples (A—the second DSC heating curves of PySMPU/OOBA complex comparing with pure OOBA and pure PySMPU; B—the DSC cooling curves of OOBA/PySMPU complexes with various OOBA contents; C—the first DSC heating curves of PySMPU/OOBA complexes with various OOBA contents; D—the second DSC heating curves of PySMPU/OOBA complexes with various OOBA contents)

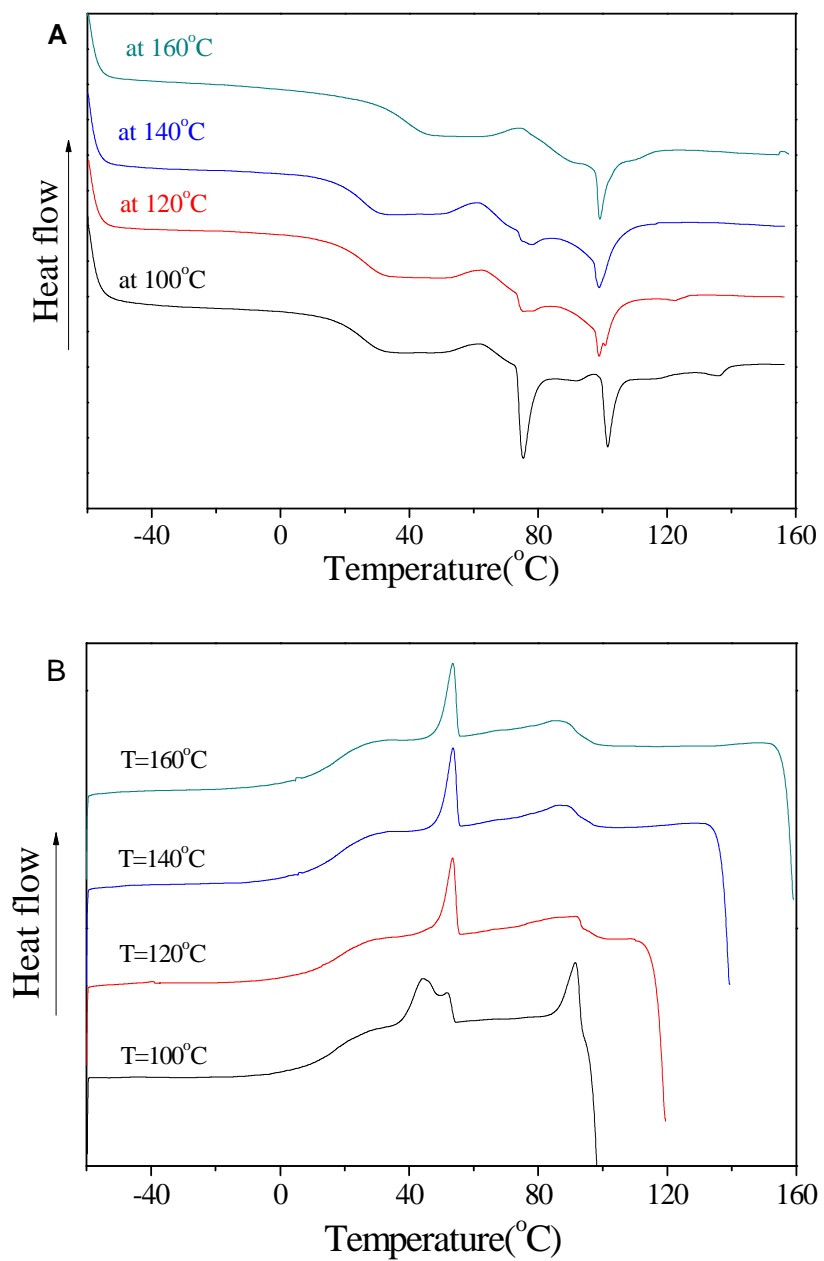


Figure 4. The heat treatment on thermal-properties of sample PySMPU-0.6OOBA (A-the second DSC heating curves; B-the DSC cooling curves)

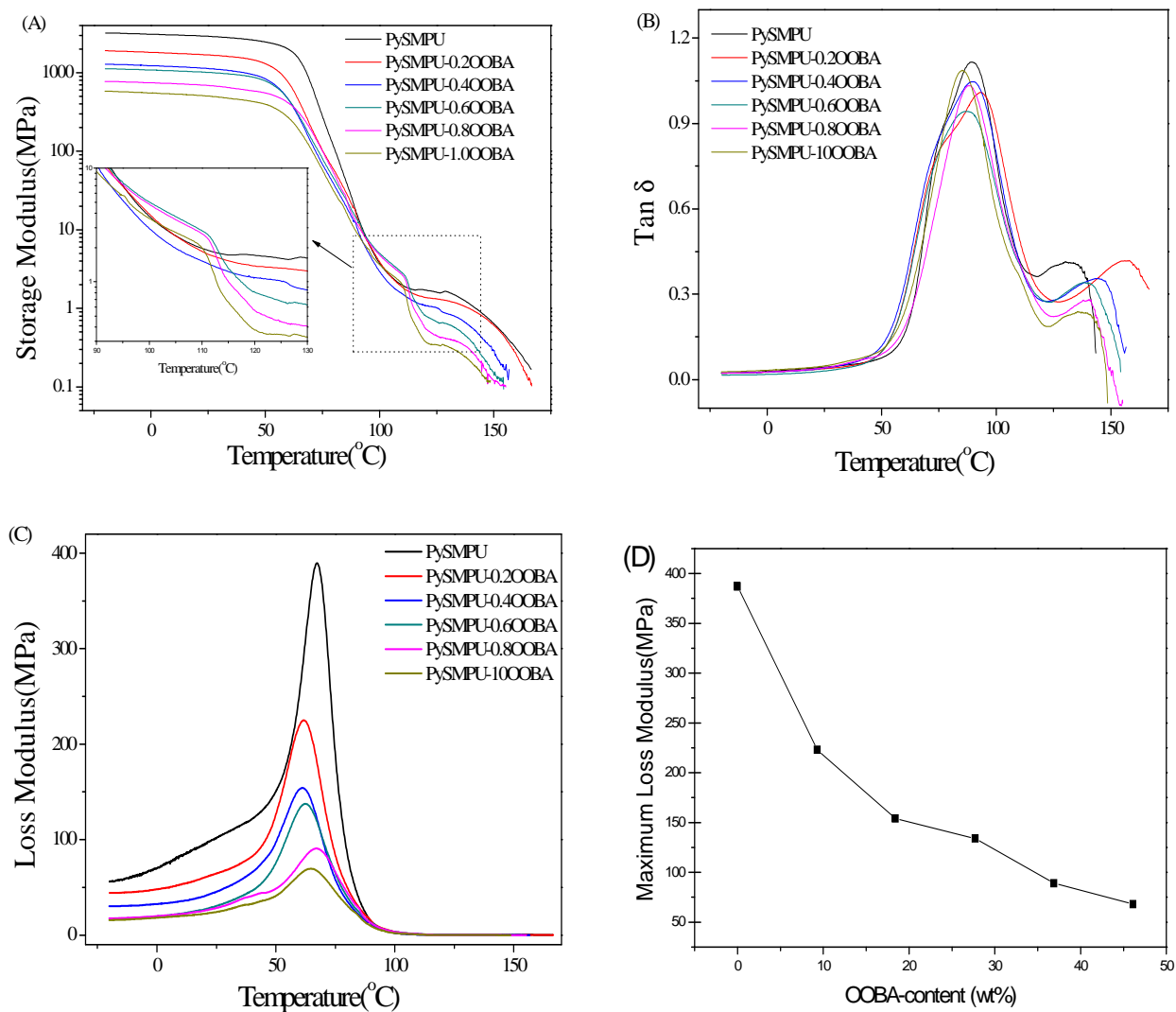


Figure 5. DMA curves of PySMPU with various OOBA (A-Storage modulus curves; B-Tan $\delta$  curves; C-Loss modulus curves; D-dependency of maximum loss modulus on OOBA-content)

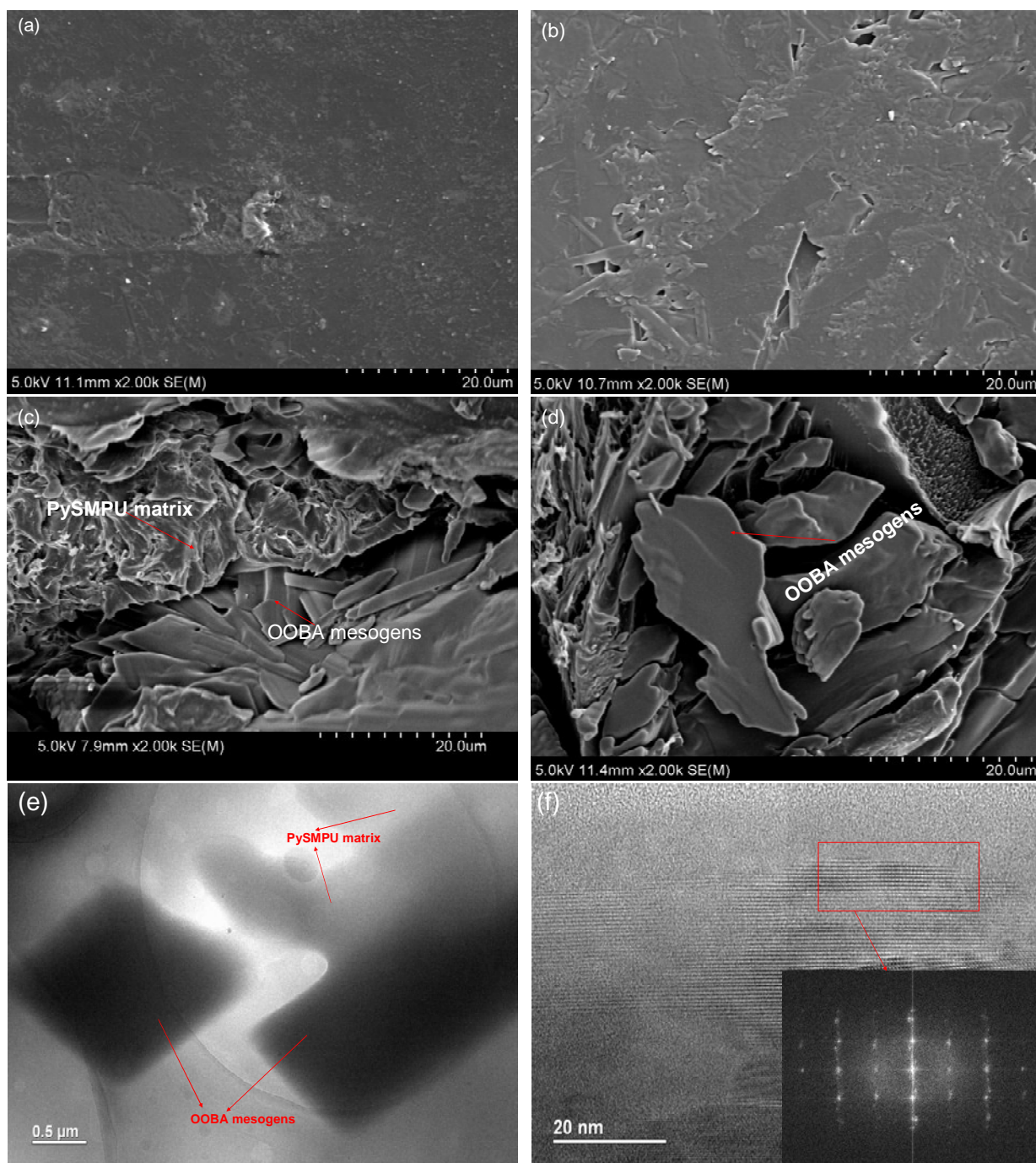


Figure 6. SEM images for ((a) surface of PySMPU; (b) surface of PySMPU-0.4OOBA; (c) broken surface of PySMPU-0.4OOBA; (d) broken surface of PySMPU-0.8OOBA) and HR-TEM images (e- for whole thin film of PySMPU-0.6OOBA; f-for crystalline region in the thin film)

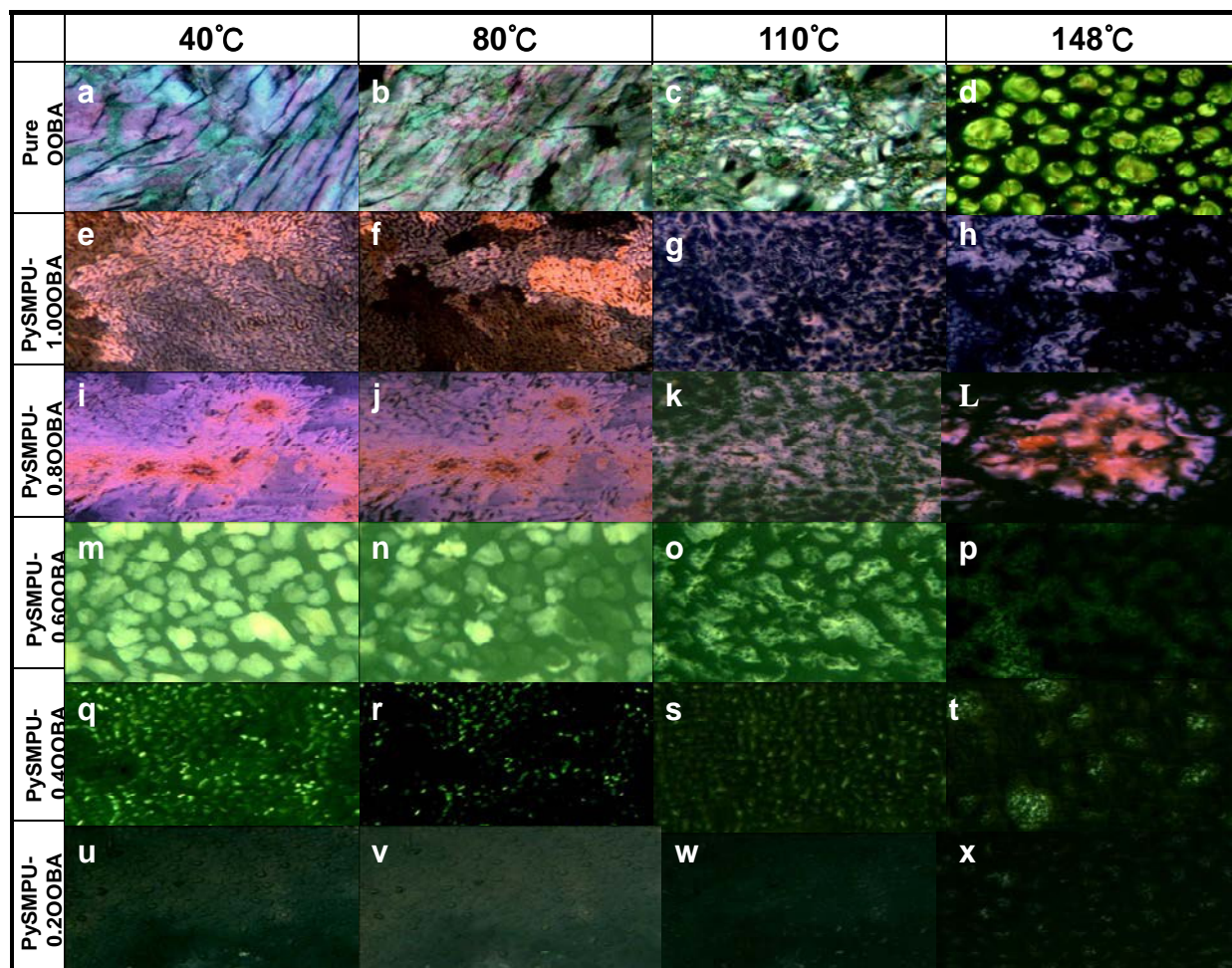


Figure 7. POM images (200 $\times$ ) of PySMPU/Ooba complex with various Ooba content at different temperature upon heating.

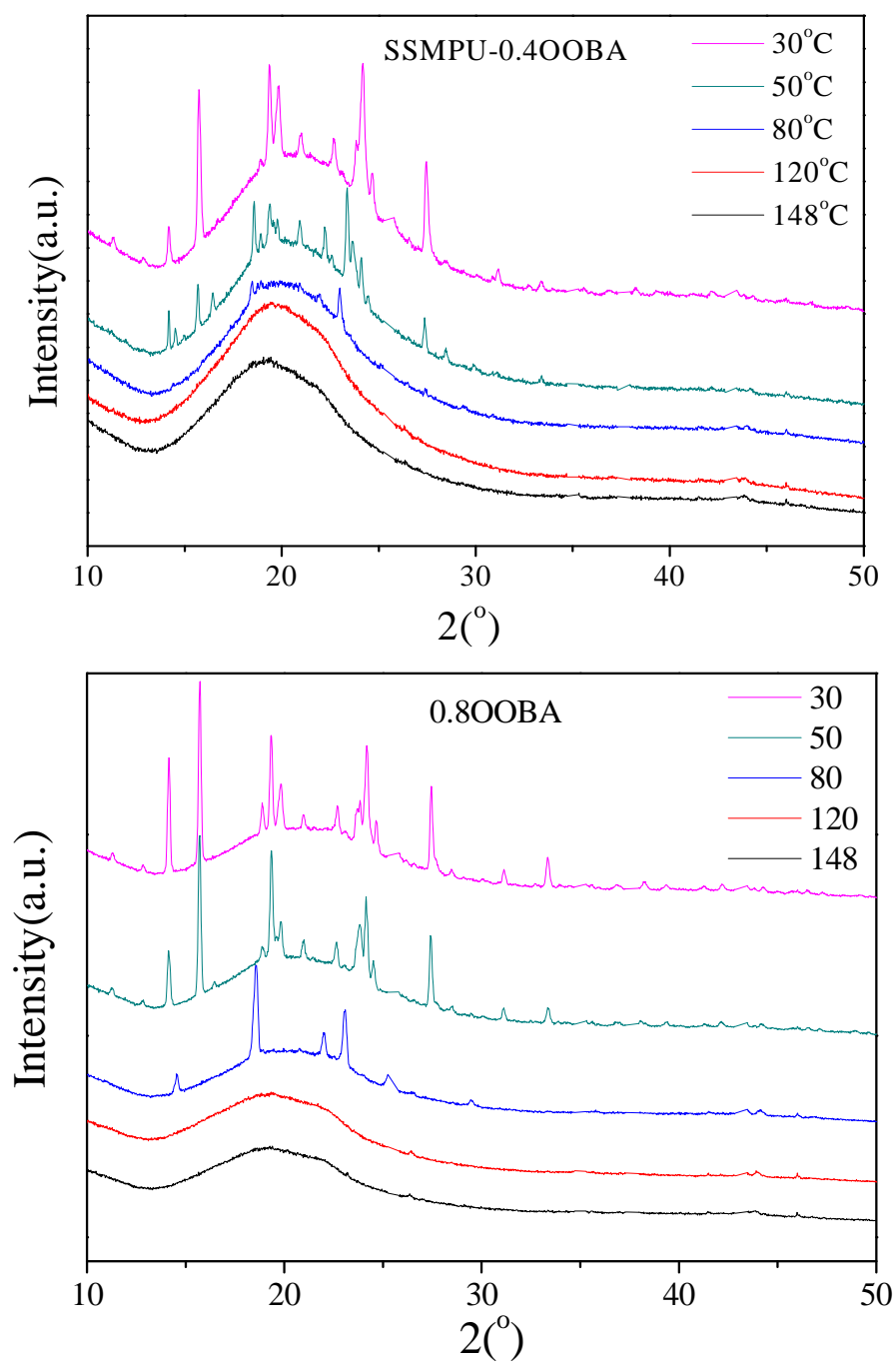


Figure 8. Variable temperature FTIR spectra of PySMPU-0.4OOBA and PySMPU-0.8OOBA

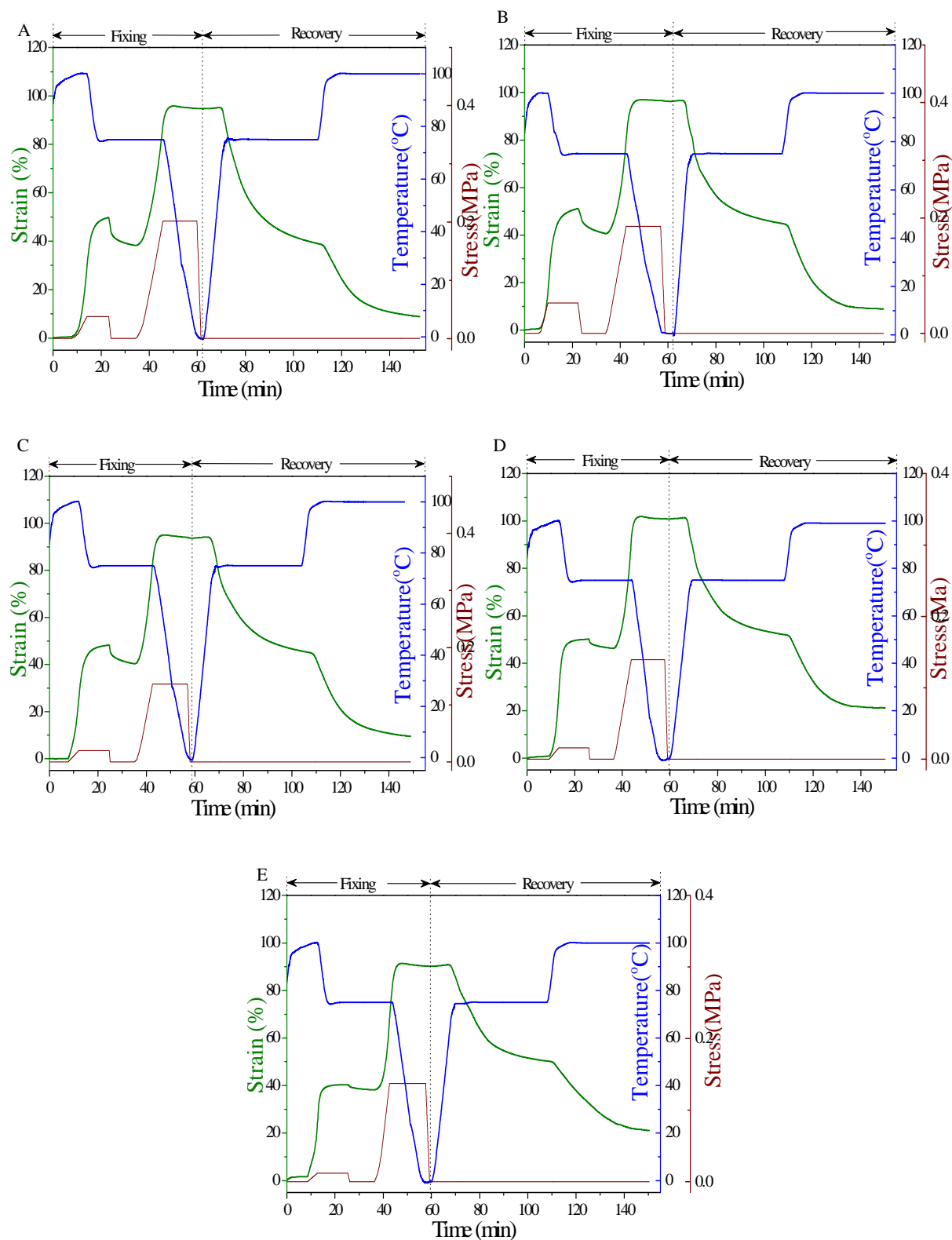


Figure 9. Triple-shape memory behaviors of PySMPU/OOBA complexes with various OOBA contents (a-PySMPU-0.2OOBA; b-PySMPU-0.4OOBA; c-PySMPU-0.6OOBA; d-PySMPU-0.8OOBA, e-PySMPU-1.0OOBA)

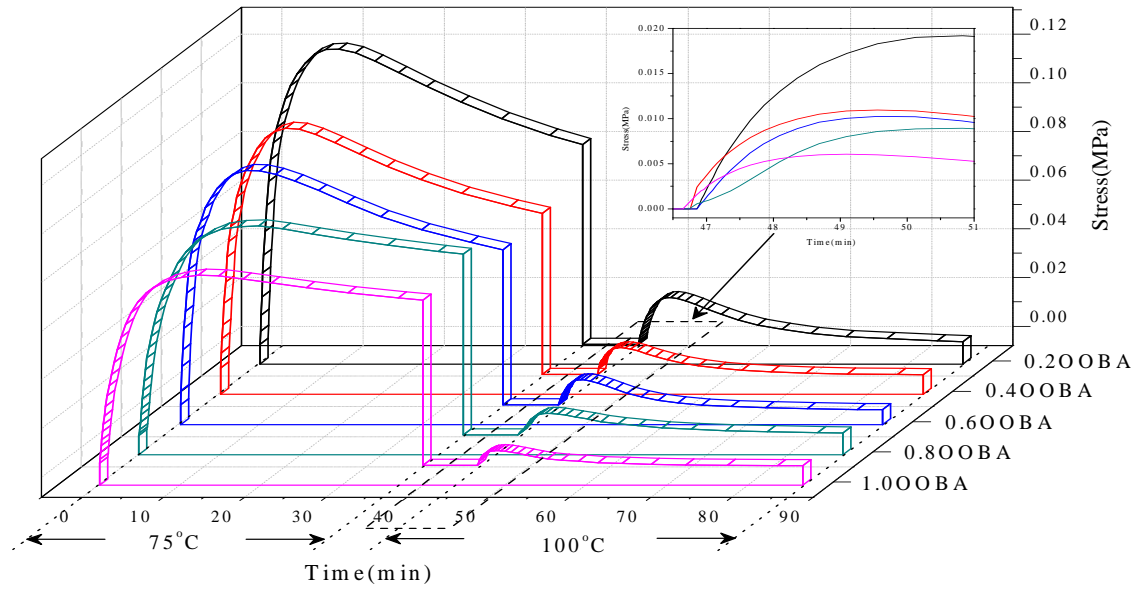


Figure 10. DMA curve for stress relaxation of PySMPU/OOBA complexes with various OOBA content

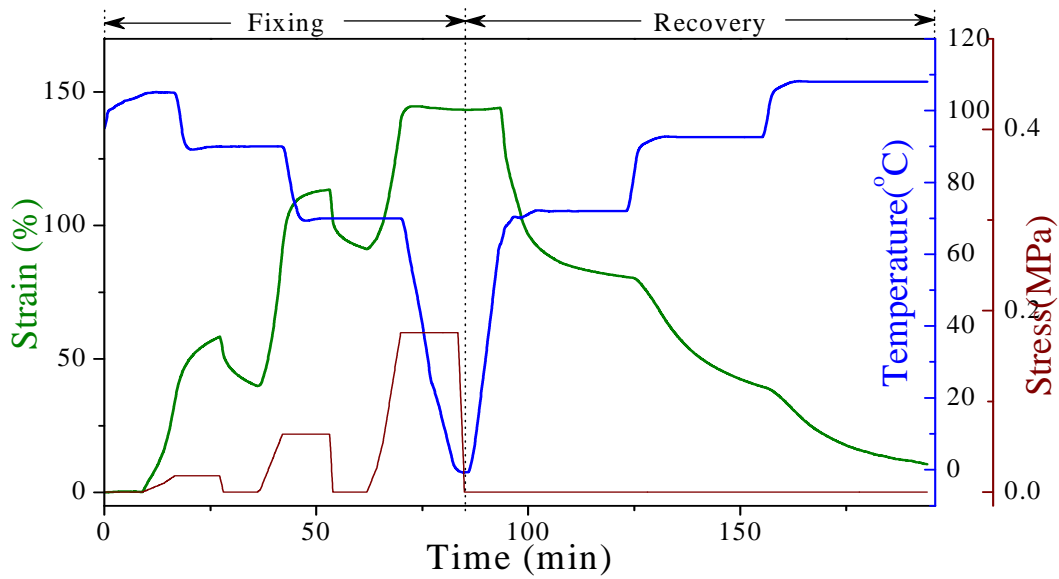


Figure 11. Quadruple-shape memory behaviors of sample PySMPU-0.2OOBA

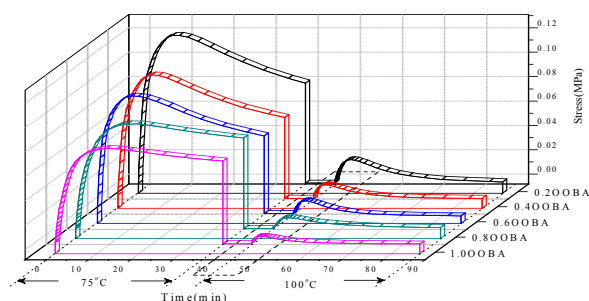
**New insights into multi-shape memory behaviours and liquid crystalline properties of supramolecular polyurethane complexes based on pyridine-containing polyurethane and 4-Octyldecyloxybenzoic acid**

Shaojun Chen<sup>1</sup>, Funian Mo<sup>1</sup>, Shiguo Chen<sup>1</sup>, Zaochuan Ge<sup>1</sup>, Haipeng Yang<sup>1</sup>, Jiandong Zuo<sup>1</sup>, Xinke Liu<sup>1\*</sup>, Haitao Zhuo<sup>2\*</sup>,

<sup>1</sup>Shenzhen Key Laboratory of Special Functional Materials, Nanshan District Key Lab for Biopolymers and Safety Evaluation, College of Materials Science and Engineering, Shenzhen University, Shenzhen, 518060, China. <sup>2</sup> College of Chemistry and Chemical Engineering, Shenzhen University, Shenzhen, 518060, China.

Corresponding authors: College of Materials Science and Engineering, Shenzhen University, Shenzhen, 518060, China. E-mail: X.K. Liu [xkliu@szu.edu.cn](mailto:xkliu@szu.edu.cn); H.T.Zhuo, [haitaozhuo@163.com](mailto:haitaozhuo@163.com)

**For Table of Contents use only**



This paper develops a supramolecular liquid crystalline complex exhibiting a multi-shape memory effect and liquid crystalline properties. Overall, increasing the mesogen content improves the strain fixity but reduces the strain recovery. The strain fixity at the first stage is lower than that at the second stage, while the strain recovery at the first stage is higher than that at the second stage.